AD-A114 107 PENNSYLVANIA STATE UNIV UNIVERSITY PARK APPLIED RESE--ETC F/G 20/1
AN EXPERIMENTAL STUDY OF TRAVELLING-BUBBLE CAVITATION NOISE.(U)
DEC 81 M F HAMILTON, D E THOMPSON, M L BILLET N00024-79-C-6043
UNCLASSIFIED ARL/PSU/TM-81-245 NL

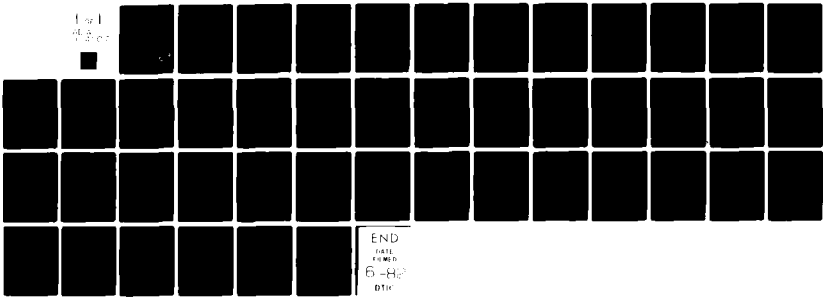

END
DATE FILMED
6-82
DTIC

AN EXPERIMENTAL STUDY OF TRAVELLING-BUBBLE CAVITATION NOISE

M. F. Hamilton, D. E. Thompson and M. L. Billet

Technical Memorandum
File No. TM 81-245
4 December 1981
Contract No. N00024-79-C-6043

Copy No. 31

The Pennsylvania State University
APPLIED RESEARCH LABORATORY
Post Office Box 30
State College, PA 16801

Approved for Public Release
Distribution Unlimited

NAVY DEPARTMENT

NAVAL SEA SYSTEMS COMMAND

SECURITY CLASSIFICATION OF THIS PAGE (When Data Entered)

REPORT DOCUMENTATION PAGE	READ INSTRUCTIONS BEFORE COMPLETING FORM
1. REPORT NUMBER: TM 81-245	2. GOVT ACCESSION NO.: AD-A114 107
	3. RECIPIENT'S CATALOG NUMBER:
4. TITLE (and Subtitle): AN EXPERIMENTAL STUDY OF TRAVELLING-BUBBLE CAVITATION NOISE	5. TYPE OF REPORT & PERIOD COVERED: Technical Memorandum
	6. PERFORMING ORG. REPORT NUMBER:
7. AUTHOR(s): M. F. Hamilton, D. E. Thompson, and M. L. Billet	8. CONTRACT OR GRANT NUMBER(s): N00024-79-C-6043
9. PERFORMING ORGANIZATION NAME AND ADDRESS: Applied Research Laboratory, Post Office Box 30, State College, PA 16801	10. PROGRAM ELEMENT, PROJECT, TASK AREA & WORK UNIT NUMBERS:
11. CONTROLLING OFFICE NAME AND ADDRESS: Naval Sea Systems Command, Department of the Navy, Washington, DC 20362	12. REPORT DATE: 4 December 1981
	13. NUMBER OF PAGES: 39
14. MONITORING AGENCY NAME & ADDRESS (if different from Controlling Office)	15. SECURITY CLASS. (of this report): UNCLASSIFIED
	15a. DECLASSIFICATION/DOWNGRADING SCHEDULE:

16. DISTRIBUTION STATEMENT (of this Report)

Approved for public release. Distribution unlimited
Per NAVSEA - April 20, 1982.

17. DISTRIBUTION STATEMENT (of the abstract entered in Block 20, if different from Report)

18. SUPPLEMENTARY NOTES

- Figure 1 (cp(min))

19. KEY WORDS (Continue on reverse side if necessary and identify by block number)

H/F, travelling, bubble, cavitation, noise

20. ABSTRACT (Continue on reverse side if necessary and identify by block number)

In this investigation, high-frequency travelling-bubble cavitation noise generated on a Schiebe headform is analyzed with regard to noise theories which are based on the collapse of a single bubble. After normalizing the noise level by an event rate, $-\sigma/C_{p_{min}}$ appears to provide a reasonable scaling factor for the noise level radiated per collapse, where σ is the cavitation number and $C_{p_{min}}$ is the minimum pressure coefficient on the headform. At

DD FORM 1 JAN 73 1473 EDITION OF 1 NOV 65 IS OBSOLETE

C-1

20. frequencies above 10 kHz and for free-stream flow velocities between 9.1 and 12.2 mps (30 and 40 fps), the noise level per collapse varied as roughly $\sigma^{-8.4}$, and was constant with the flow velocity for constant $-\sigma/C_{p_{min}}$. The energy density spectra were flat from 10 to 100 kHz regardless of the cavitation number or free-stream velocity.

Subject: An Experimental Study of Travelling-Bubble Cavitation Noise

References: See page 27.

Abstract: In this investigation, high-frequency travelling-bubble cavitation noise generated on a Schiebe headform is analyzed with regard to noise theories which are based on the collapse of a single bubble. After normalizing the noise level by an event rate, $-\sigma/C_{p_{min}}$ appears to provide a reasonable scaling factor for the noise level radiated per collapse, where σ is the cavitation number and $C_{p_{min}}$ is the minimum pressure coefficient on the headform. At frequencies above 10 kHz and for free-stream flow velocities between 9.1 and 12.2 mps (30 and 40 fps), the noise level per collapse varied as roughly $\sigma^{-8.4}$, and was constant with the flow velocity for constant $-\sigma/C_{p_{min}}$. The energy density spectra were flat from 10 to 100 kHz regardless of the cavitation number or free-stream velocity.

Acknowledgement: This work was performed at the Applied Research Laboratory under the sponsorship of the Naval Sea Systems Command, Acoustical Silencing Program, PE 62543N, Subproject SF 43-452, Task 452-150-100. The authors would also like to acknowledge the helpful comments of Mr. H.-J. Baiter at the Fraunhofer-Institut für Hydroakustik, Ottobrunn, West Germany. This paper has been submitted for presentation at the ASME Symposium on Cavitation Noise to be held at Pheonix, Arizona in November 1982.

Table of Contents

List of Figures

NOMENCLATURE

a	radius of Schiebe body
c	speed of sound
C_p	pressure coefficient
$\overline{C}_p$	average pressure coefficient where $P < P_v$
$C_{p_{min}}$	minimum pressure coefficient
f	frequency
L	noise level
L_c	noise level per collapse
M	shock wave parameter
N	number of collapses per second
p	acoustic pressure
P	pressure
P_g	noncondensable gas pressure
P_s	peak shock wave pressure
P_v	vapor pressure
P_∞	free-stream static pressure
r	radial coordinate
R	bubble radius
$\dot{R}$	bubble wall velocity
$\ddot{R}$	bubble wall acceleration
R_m	minimum bubble radius
R_M	maximum bubble radius
s	length on surface of Schiebe body
s_v	length of region where $P < P_v$
S	spectral energy density
t	time

NOMENCLATURE (Cont'd)

V	bubble volume
$\ddot{V}$	second derivative of bubble volume
V_∞	free-stream velocity
θ	time constant
ρ	mass density of water
σ	cavitation number
σ_d	desinent cavitation number
σ_i	incipient cavitation number
τ	bubble collapse time

INTRODUCTION

Although there have been many experimental investigations of cavitation noise, most studies are generally concerned with well-developed forms such as wake, vortex or fixed-patch cavitation. In those cases, the entire cavitating region is regarded as a single complex noise source as opposed to considering the collapse of each individual bubble. Near inception when the bubbles are collapsing independently, the radiated noise is often more intense than when the cavitation becomes developed. Such incipient cavitation noise has already been analyzed - for example on hydrofoils by Barker [1] and Blake et. al. [2] - but because of the typically narrow ranges of flow parameters which support incipient conditions, relations indicating how the noise depends on the flow parameters have not been determined for these cases. Noise studies have also been conducted for the collapse of a single bubble. This was accomplished by Harrison [3], Mellen [4], and more recently by Chahine et. al. [5] where spark gaps were used to generate the bubbles, and also by Hentschel [6] who employed a focused laser beam for that purpose. However, the parameters involved in those investigations do not reflect those typically encountered in flow-induced cavitation.

Therefore, the present study examines travelling-bubble cavitation which is easily generated on a Schiebe headform. In travelling-bubble cavitation each bubble collapses independently, while the Schiebe headform allows for a relatively wide operating range, in terms of flow parameters, for this type of cavitation to exist. Measurements of cavitation noise generated in this way are compared to the relevant theories for noise radiation due to bubble collapse.

Cavitation noise analysis essentially began in 1917 with Rayleigh's solution [7] to the problem posed by Besant [8] of calculating the pressure field generated by the collapse of a spherical cavity in an incompressible fluid. The extension of this analysis by Plesset [9] resulted in the Rayleigh-Plesset equation governing the dynamics of a bubble in an arbitrary time-varying pressure field. It has been shown [10] how this classical analysis predicts an energy spectrum which rises as roughly f^4 to a peak at a frequency near the reciprocal of the bubble lifetime, after which it rolls off as $f^{-2/5}$. Both Mellen [11] and Blake et. al. [2] obtained noise spectra which exhibited this type of spectral response, except that their roll-offs behaved as f^{-2}.

Subsequent theoretical advances in modelling cavitation noise were few and far between. Not until World War II was an analysis of the propagation of weak shocks developed by Kirkwood and Bethe [12] which enabled Gilmore [13] in 1952 to derive an equation for the collapse of a bubble in a compressible fluid. Both experiment [4] and numerical analysis [14] have demonstrated the accuracy of Gilmore's theory, particularly around the final stage of collapse where bubble wall velocities are sonic and the effects of compressibility become important. However, solutions of that equation must be obtained by numerical methods, and as such it does not yield useful analytical predictions of the radiated sound field.

Another important parameter during the final collapse stage is the presence of any noncondensable gas contained in the bubble. In addition, acoustic pressure waves may be generated by the high bubble wall velocities. Using Whitham's method [15] of describing shock wave propagation, Baiter [16] recently derived an expression for the pressure pulse in the far field of the bubble, including the effects of noncondensable gas pressure but not of compressibility with respect to bubble dynamics. Esipov and

Naugol'nykh [17], using the Kirkwood-Bethe approximation, did include the effects of compressibility and arrived at a solution similar to Baiter's. Both solutions assume a shock wave having an exponential profile, and consequently depict a flat energy spectrum which eventually rolls off at the high end around a frequency determined by the time constant of the wave profile. A number of experiments [1,2,11] yielded noise spectra which hinted at such a high frequency spectral plateau.

Thus, this investigation will relate these noise theories to the sound radiated by travelling-bubble cavitation. Comparisons are based on how the noise level per collapsing bubble depends on the cavitation number σ and the flow velocity V_∞. The independent behavior of the bubbles permits the measured frequency spectra to be compared with those predicted by the single bubble noise theories [18].

EXPERIMENTAL APPARATUS AND PROCEDURE

This investigation was conducted in the 305 mm (12 in.) diameter water tunnel of the Applied Research Laboratory at the Pennsylvania State University. The headforms used were two 50.8 mm (2 in.) diameter Schiebe noses which were identical except for modifications that provided measurements of either static or acoustic pressure. Schiebe headforms do not experience laminar separation, and they support travelling-bubble cavitation for a relatively wide pressure range provided there are enough microbubbles available in the free stream [19].

To measure the pressure distribution along the surface of the Schiebe nose, one headform was equipped with ten flush-mounted pressure taps at various distances from the stagnation point. These pressures were compared with the free-stream static pressure, for flow velocities ranging from 6.1 to 18.3 mps (20 to 60 fps), to determine the pressure coefficient C_p defined as

$$C_p = \frac{P - P_\infty}{\frac{1}{2}\rho V_\infty^2} \quad . \tag{1}$$

With the cavitation number σ given by

$$\sigma = \frac{P_\infty - P_v}{\frac{1}{2}\rho V_\infty^2} \quad , \tag{2}$$

measurements of the incipient and desinent cavitation numbers, σ_i and σ_d respectively, were determined visually with the aid of a stroboscope by adjusting the test section pressure at constant flow velocities. Attempts to use the cavitation noise to define these quantities are described in Reference [20], but those approaches were unreliable.

A study of bubble dynamics was accomplished with a high-speed photographic system which consisted of a Redlake Hycam camera and an EG & G type 501 stroboscope. The Hycam is a 16 mm rotating prism camera which was adjusted to a framing rate of roughly 1800 pictures per second. A Schiebe nose was modified with a small barium-titanate transducer which was mounted flush with the surface of the model 60 mm downstream from the stagnation point. Thus, at the same time that the high-speed films of bubble collapse were taken, the resulting noise was being monitored by that transducer. After high-pass filtering at 10 kHz, the noise was recorded on a Bell and Howell type CPR-4010 tape recorder. The tape recording was synchronized with the films via voltage spikes input to a second channel which marked the points in time where the strobe would fire to create each successive picture.

Additional studies of bubble dynamics were realized by filming the cavitation on videotape. Voltages corresponding to the pressure and

velocity in the test section were called out and recorded on the audio track of the tape so that the effects of a wide range of flow parameters could be observed.

To measure the cavitation noise level, a 25 mm (1 in.) diameter lead-zirconate-titanate (PZT) hydrophone was coupled to the outside of the test section window. The specific acoustical impedance of the window was near that of water such that minimum sound reflection occurred at the interface formed by the two media. The hydrophone was aimed at a location on the model about 50 mm downstream from the stagnation point. With a separation of about 150 mm (6 in.) between the face of the hydrophone and the surface of the model, the measured beamwidth on that surface was about 70 mm at its half-power points.

After high-pass filtering at 10 kHz, the output from the hydrophone was input to one channel of the tape recorder. A DC voltage output from an rms voltmeter, which represented the cavitation noise level above 10 kHz, was input to a second channel. On yet a third channel was recorded a DC voltage which was proportional to the free stream static pressure in the test section. The entire arrangement is illustrated in Figure 1.

Tests were run at flow velocities ranging from 9.1 to 12.2 mps (30 to 40 fps) in increments of 0.76 mps (2.5 fps). With the velocity held constant, the pressure in the test section was lowered from an initial point above σ_i. As soon as noise bursts due to bubble collapse were witnessed on an oscilloscope, tape recording would begin as the pressure was continuously lowered until the travelling-bubble cavitation transformed into an attached cavity. This procedure was repeated at each velocity. In addition, noise spectra from 10 to 100 kHz were obtained

using a Celesco LC-10 hydrophone mounted in a parabolic reflection dish on the test section window. Adjustments for natural resonances due to the test section geometry were made on the basis of spectra generated by a calibrated LC-10 source located adjacent to the model. The spectra were analyzed with a Spectral Dynamics SD-360 real time FFT processor.

Finally, the effect of the velocity and pressure on the sound transmission path was investigated. The temperature of the water used throughout this investigation was approximately 21°C, while the total gas content was roughly 10 parts per million (PPM) air to water on a molar basis as measured with a van Slyke apparatus. To determine how sound was absorbed by free-stream bubbles as a function of pressure, white noise was projected into the test section through the window opposite the PZT hydrophone. This test was conducted at 7.6 mps (25 fps) since lower pressures are required to support cavitation at correspondingly lower velocities, and hence any effects due to free-stream bubbles should be prevalent under these conditions. Attenuation of less than 1 dB was observed above 10 kHz after lowering the pressure from a state of no cavitation until the cavitation noise itself obscured the projected white noise. Consequently, this effect was ignored.

There were essentially two reasons for high-pass filtering all noise measurements at 10 kHz. First, the water tunnel itself generated so much noise at low frequencies as to render making adjustments for the background noise almost impossible. Second, near-field effects make interpretation of measurements below 10 kHz questionable. The wavelength of sound in water at that frequency is already about 150 mm (6 in.), which is approximately the distance from the region of cavitation to the hydrophone.

MATHEMATICAL MODELS

The dynamics of a spherical bubble in an incompressible fluid are described by the Rayleigh-Plesset equation [9],

$$R\ddot{R} + \frac{3}{2}\dot{R}^2 = \frac{P(R) - P_\infty}{\rho} \tag{3}$$

where $P(R)$ represents the pressure applied by the contents of the bubble to the bubble wall located at radius $R = R(t)$, and P_∞ is the pressure field experienced by the bubble. Very often $P(R)$ is considered to be constant and equal to the vapor pressure of water, P_v. This approximation becomes unacceptable only at the very beginning and end of the bubble life cycle where gas content must be considered for small bubble volumes. Also, effects of viscosity and surface tension have been shown to exert only a minor influence on bubble dynamics [21].

Equation (3) yields several analytical expressions describing various stages of growth and collapse for a bubble in a local pressure field defined by P. During vaporous bubble growth, it can be shown [22] that the bubble wall velocity remains essentially constant. Thus, setting $\ddot{R} = 0$ and $P(R) = P_v$ in Equation (3), an approximate formula for the maximum bubble radius R_M is easily derived and given by

$$R_M = s_v \sqrt{\frac{1}{3}\frac{\overline{C}_p + \sigma}{\overline{C}_p - 1}} \quad , \tag{4}$$

where s_v is the length of the bubble path along which $P < P_v$. It is assumed here that bubble growth occurs only in that region, with the average pressure represented by $\overline{C}_p$.

Even during collapse, the noncondensable gas pressure becomes significant only for $R << R_M$. However, at this point the bubble wall velocity is so

high that it violates the assumption of incompressibility, invalidating Rayleigh's analysis. Nevertheless, Rayleigh calculated the collapse time of a bubble for $P(R) = P_v$ to be

$$\tau = 1.3 \frac{R_M}{V_\infty \sqrt{C_p + \sigma}} \quad . \tag{5}$$

Hickling and Plesset [14] have shown Equation (5) to agree within 1% of their numerical analysis for a compressible liquid in the absence of any vapor pressure.

In the far field of the bubble, the Rayleigh-Plesset equation yields input for calculating the acoustic pressure [23]

$$p(r,t) = \frac{\rho}{4\pi r} \ddot{V}(t - \frac{r}{c}) \quad , \tag{6}$$

where $V = (4/3)\ \pi R^3$ is the bubble volume. Using the Rayleigh-Plesset equation again to derive an asymptotic expression for the radius R(t) of a collapsing bubble for $R << R_M$, the acoustic pressure becomes

$$p(r,t) \alpha \left[\frac{\rho}{r}\right] V_\infty^{6/5} R_M^{9/5} (C_p + \sigma)^{3/5} t^{-4/5} \quad . \tag{7}$$

Taking the Fourier transform of Equation (7) and squaring the result, the energy density is then

$$S(f) \alpha \left[\frac{\rho}{r}\right]^2 V_\infty^{12/5} R_M^{18/5} (C_p + \sigma)^{6/5} f^{-2/5} \quad . \tag{8}$$

Any noncondensable gas contained in a bubble cushions the collapse and for small amounts of gas the collapsing bubble can rebound into another growth stage. This requires an abrupt change in the movement of the

surrounding fluid and produces a compression wave. This compression wave propagates outwards and can possibly form a shock front. Shock formation is caused by nonlinear compressibility effects on sound radiation. It occurs when the initial pulse amplitude is high enough so that the shock is formed before the nonlinear effects are neutralized through geometric attenuation and propagation losses. Assuming that an exponentially shaped shock wave occurs, Baiter [16] followed Whitham's analysis [15] and derived

$$p(r,t) = P_s \, e^{-t/\theta} \quad , \tag{9}$$

to arrive, via the Rayleigh-Plesset equation, at values of P_s and θ given by

$$P_s \propto \rho c^2 \frac{R_M}{r} \left(\frac{P_g}{\rho c^2}\right)^{1/4} \left(\ell n \frac{r}{R_n}\right)^{-1/2} \tag{10}$$

and

$$\theta = 5.9 \frac{R_M}{c} \left(\frac{P_g}{\rho c^2}\right)^{1/4} \left(\ell n \frac{r}{R_m}\right)^{1/2} \quad . \tag{11}$$

R_m is the minimum radius of the bubble at the instant where rebound occurs, and P_g refers to the gas pressure in the bubble when $R = R_M$. The above relations require $P_g \ll P$ for a gas behaving adiabatically with a specific heat ratio equal to 4/3.

Considering again a noncondensable adiabatic gas but accounting for compressibility of the fluid, Esipov and Naugol'nykh [17] used the Kirkwood-Bethe approximation [12] to arrive at an expression in the form

of Equation (9) where the pressure is again given by Equation (10), but now

$$\theta = \frac{R_M}{c}\left(\frac{P_g}{\rho c^2}\right)^{1/4}\left[M^{-3/2} + 2\sqrt{2}\left(\ell n\,\frac{r}{R_m}\right)^{1/2}\right] \quad . \tag{12}$$

They define the parameter M as

$$M = \left[\frac{1}{2} + \frac{3P_g^{3/4}\,(\rho c^2)^{1/4}}{P}\right]^{-1} \quad . \tag{13}$$

Shock wave pulses are often modelled by an exponential pulse. The energy density spectrum of Equation (9) is

$$S(f) = \frac{(P_s\theta)^2}{1 + (2\pi\theta f)^2} \quad . \tag{14}$$

Equation (14) implies a flat spectrum up until a cutoff frequency given by

$$f = \frac{1}{2\pi\theta} \quad , \tag{15}$$

after which the spectrum will roll off as f^{-2}. Thus, to find the energy density below the cutoff frequency, it is sufficient to determine

$$S(f) = (P_s\theta)^2 \quad . \tag{16}$$

For the range of flow parameters used in this investigation, the bubbles experience pressures between 0.2 and 0.5 atm during their collapse stage. Consequently, the $M^{-3/2}$ term in Equation (12) may be neglected for $P_g < 0.001$ atm. In fact, such low gas pressure is required for using

Equations (9) through (12) because of the assumption that shock formation does indeed occur. Hickling and Plesset (14) showed that, with a pressure of 1 atm forcing collapse, shock formation just barely occurs for an initial gas pressure of 0.01 atm. Higher gas pressures will cushion the collapse sufficiently to prohibit shock formation altogether. Thus, Equation (12) becomes almost identical to Equation (11) so that the energy density below cutoff becomes, from Equation (16),

$$S(f) \propto \frac{\rho}{r^2} R_M^4 P_g \quad . \tag{17}$$

RESULTS AND DISCUSSION

The shape of a Schiebe headform is determined by the profile of streamlines resulting from the addition of a disk source to a uniform flow field [24]. As such, no closed-form solution describing the pressure distribution along its surface exists, so a computer-generated solution appears in Figure 2. Distance along the surface of the headform is measured by the dimensionless quantity s/a, where the actual length s is normalized by the maximum radius of the model. In this case, that radius is a = 25.4 mm (1 in.). The experimental values of C_p appearing in Figure 2 result from averaging a number of runs through the range of flow velocities. An uncertainty of ±0.01 is associated with each point.

Figure 3 gives values obtained for the incipient and desinent cavitation numbers, σ_i and σ_d respectively, with an uncertainty of ±0.03. The error is often larger at lower velocities where the free-stream pressure must correspondingly be lower to cause cavitation. At those lower pressures, free-stream air bubbles can become large enough to be confused with cavitation on the model.

The point at which travelling-bubble cavitation abruptly transforms into an attached cavity is denoted in Figure 3 by Attached Cavity σ_i. Note that this parameter remains relatively constant for different velocities. Thus, as the velocity increases, the operating range of pressure that can support travelling-bubble cavitation diminishes. This established 12.2 mps (40 fps) as a practical upper limit for the flow velocity where meaningful trends of noise versus pressure could be measured.

An interesting feature of Figure 3 results from a comparison with Figure 2. Classical theory predicts $\sigma_i = \sigma_d = -C_{p_{min}}$ for vaporous cavitation, implying that vaporous cavitation should not exist for any $\sigma > -C_{p_{min}}$ as there is then no location on the model where $P \leq P_v$. With $C_{p_{min}} = -1.0$ on the headform, an alternative type of cavitation above $\sigma = 1.0$ must be suggested to account for the values of σ_i and σ_d at velocities below 11.4 mps.

The most probable cause for this discrepancy is that the cavitation nuclei contain gas having pressure greater than P_v. Thus, passage through a region of local pressure less than that of the gas pressure may cause the nuclei to grow enough to be confused with vaporous cavitation. For example, $\sigma = 1.2$ at a velocity of 9.1 mps indicates a minimum pressure of about 0.1 atm on the surface of the headform, implying a gas pressure of that same value as compared with $P_v = 0.03$ atm. As the bubble grows, however, the gas pressure decreases as R^{-3} for isothermal expansion or as R^{-4} if the expansion is adiabatic. This results from gas diffusion through the bubble wall being insignificant in relation to the rate of bubble growth and collapse. Consequently, the pressure rapidly approaches P_v and remains essentially constant during bubble growth. Thus, vaporous cavitation will dominate as the pressure is lowered.

The trend for σ_i and σ_d to decrease with increasing velocity is not uncommon at high air contents such as 10 ppm. Since this phenomenon is discussed more thoroughly in Reference [25], it is sufficient here to note that the effect of any gas content is to increase the point of inception for decreasing flow velocities. Where a specific example at 9.1 mps was shown to suggest a gas pressure of 0.1 atm, this merely set an upper bound for the gas pressure in those particular cavitation nuclei which were prone to expansion at that value of σ. Since the nuclei possess a distribution in size, those participating in cavitation inception represent the largest nuclei in the spectrum. Smaller free-stream nuclei may have lower gas pressures because of higher surface tension which resists gas diffusion through the bubble wall.

Data resulting from the high-speed films and videotapes were compared with the equations describing bubble growth and collapse. Measurements of R_M exceeded the predictions of Equation [4] by factors ranging from 2 to 4. It is interesting that Blake et. al. [2] performed similar calculations for travelling-bubble cavitation on a hydrofoil and found Equation (4) to overestimate their maximum bubble radii by about 20%. At the very least, this suggests that Equation (4) is more suited to the experiment conducted by Blake et. al., therefore inviting comparison.

A critical parameter in Equation (4) is the distance s_v travelled by the bubble where it experiences a local pressure $P < P_v$. The illustrative examples discussed in Blake's investigation [2] show s_v to be greater than 30 mm, such that the bubbles have almost attained their maximum radii by the time they leave that low pressure region. For the pressure

range encountered in the present investigation, this low pressure region extends for less than 4 mm along the Schiebe headform. Also, the high-speed films showed that bubble growth did not usually begin until about the time that the nucleus was leaving the low pressure region and most of the bubbles occurred outside of the boundary layer on the Schiebe headform.

Thus it is not surprising that the bubble growth observed by Blake et. al. is adequately modelled by Equation (4), where the growth stage was assumed to be entirely limited to the region where $P < P_v$. Yet clearly, inertial effects responding to the low pressure impulse are primarily responsible for growth on the Schiebe headform. What is not certain is whether Equation (4) correctly describes the functional dependence of R_M on σ and C_p despite an inability to predict specific values.

Similarly, measurements of collapse times were compared with the predictions of Equation (5). The measured times were generally longer than those calculated using Equation (5) by a factor of 2 to 3, while Blake et. al. observed collapse times only 15% in excess of the predicted values. Air content is one basic difference here; Blake et. al. held the air content below 2.5 ppm, but in this investigation it was approximately 10 ppm. Higher air content yields an increased noncondensable gas content which will retard the rate of collapse, while Equation (6) assumes the pressure in the bubble to be constant and equal to P_v. It is interesting that Harrison [3], observing bubble cavitation in a venturi nozzle where he maintained an air content of about 5 ppm, recorded data for bubble collapse corresponding exactly to Rayleigh's theory.

A second difference is the shape of the pressure curve on the body. The Schiebe headform has a very steep rise in pressure downstream of the location of the minimum pressure. This can be contrasted to a gentle rise in pressure downstream of the location of the minimum pressure on the hydrofoil used by Blake et. al. Equation (5) estimates the collapse time on the assumption of an averaged constant pressure; but to be realistic, one must allow for a changing pressure.

As verified repeatedly in previous investigations, the high-speed films showed sound radiation occurring at the final instant of collapse. Only a few rebounds were observed at 7.6 mps (25 fps), while none were directly observed at higher velocities. Although those runs were all performed at an air content of 10 ppm, additional films were obtained at 7.6 mps with an air content of 5 ppm. Under these conditions rebounding was frequent with significant sound generated by the collapse of the rebound. In fact, Chahine et. al. [5] observed pressure pulses due to the collapse of rebounds that were as large and sometimes even larger than the pulse from the initial collapse. The results they cited were for spark-induced bubbles collapsing at a distance less than the maximum bubble diameter away from a rigid wall. Cavitation on headforms occurs well within that proximity, so that cavitation noise theories should account for this phenomenon once rebounding becomes significant.

The noise radiation per bubble collapse was analyzed by digitizing tape recordings of the cavitation noise and viewing the output on an oscilloscope. Digitization was performed at an effective sampling rate of 200 kHz such that the acoustic signal was analyzed for continuous intervals of 185 msec in real time. For each time segment, the noise

level and pressure in the test section were determined by voltages recorded on separate channels, which were sampled immediately before and after every 185 msec interval. Thus, by counting the number of noise bursts occurring in each segment, the manner in which the noise level per collapse depended on the pressure was determined. This procedure was repeated at different velocities.

It should be noted that this measured event rate is not necessarily the same as the number of cavitation bubbles being created at that time. However, acoustic reflections off the tunnel walls were found to be insignificant by observing the response of acoustic impulses generated in the test section. Also, since the noise tests were conducted at velocities between 9.1 and 12.2 mps where the high-speed films and videotapes indicated negligible rebounding action, this factor was ignored. Finally, the collapse of some bubbles may be accompanied by an insignificant sound output, but these cases were assumed to represent anomalous behavior. Thus it may be assumed that the number of noise bursts adequately represents the actual number of cavitation bubbles. More importantly, good relations for the noise per collapse are obtained which can then be compared with the relevant theories. In what follows, it is assumed that each noise burst counted represents a single collapse.

Accordingly, the number of collapses per second, N, appears in Figure 4 as a function of pressure and velocity. The cavitation number σ is normalized by σ_d and plotted on a logarithmic scale. Lines drawn through the data at each velocity to fit the majority of points in a mean square sense yield slopes which are quite similar, having as an average functional relationship $N \alpha \sigma^{-10.6}$. Similarly, Figure 5 displays the data representing the dependence of the total noise level, L, on

pressure and velocity. Again the lines drawn through the data possess similar slopes, which yield the average relationship $L \alpha \sigma^{-19.0}$. The uncertainty in the exponents is ±1.8.

Thus, although the noise level increases rapidly as the pressure is lowered, so does the rate of bubble collapse. Figure 5 shows that the noise tends toward a saturation level for very low pressures. Such a trend is also observed to a lesser extent in Figure 4 where the collapse rate appears to level off shortly before the abrupt transition into an attached cavity.

Although normalization by σ_d in Figures 4 and 5 spread out the data for clearer presentation, it was initially thought that σ/σ_d, or equivalently σ/σ_i, would serve as an appropriate scaling factor for the noise per collapse. The reason that this is not the case relates to the discussion of why σ_i and σ_d are not constant in Figure 3 where predominantly gaseous cavitation was assumed to exist above $\sigma = 1.0$ at all velocities. This does not mean that nuclei with gas pressures as high as 0.1 atm will not give rise to bubbles that will eventually collapse with sufficient violence to generate appreciable sound. After all, for adiabatic expansion the nuclei need only grow to a maximum radius just over three times their initial radius to attain $P_g = 0.001$ atm at $R = R_M$, such that shock formation is almost inevitable. However, since gaseous bubble growth is not nearly as explosive as that of vaporous cavitation, cavitation above $\sigma = 1.0$ may indeed produce negligible sound output. In view of this, it is not surprising that the noise does not scale with σ_d. Instead, $-C_{P_{min}}$ was chosen to be the normalization factor since it corresponds in theory to the values of σ marking vaporous cavitation inception.

Therefore, the curves in Figures 4 and 5 are plotted again in Figures 6 and 7 against $-\sigma/C_{p_{min}}$, where $-C_{p_{min}}$ seems a reasonable choice for the normalization factor. In fact, the curves for the total noise level in Figure 7 appear to have collapsed quite well. The somewhat greater scatter associated with the curves in Figure 6 may simply be a reflection of the difficulties inherent in counting the noise bursts, especially with increasing cavitation activity.

The choice of $-C_{p_{min}}$ for the normalizing factor is based on the theory that vaporous cavitation begins at values of σ corresponding to $-C_{p_{min}}$. To further verify this choice of normalizing factors, a series of tests should be conducted, following the present scenario, with a series of bodies having different values of $C_{p_{min}}$. Correlation of the results using $-C_{p_{min}}$ would then establish its validity as the proper normalizing factor.

To derive relationships for the noise level per collapse, L_c, the curves fitting the data for each velocity in Figure 7 were normalized by the corresponding curves in Figure 6. The resulting curves are displayed in Figure 8 where the slopes suggest the average relationship $L_c \alpha \sigma^{-8.4}$, with an uncertainty of ±2.5 in the exponent. The salient feature of Figure 8 is that the noise per collapse appears to scale with $-\sigma/C_{p_{min}}$ alone, with apparently no contribution from V_∞. Thus, for each free-stream velocity, the functional dependence of the noise on $-\sigma/C_{p_{min}}$ is roughly the same. Additionally, the dependence of σ itself on V_∞ is such that for a constant value of $-\sigma/C_{p_{min}}$, the noise per collapse is practically equivalent for any value of V_∞.

Aside from difficulties in counting the noise bursts, another possible reason for the scatter of the slopes in Figure 8 is that the conditions in the tunnel change slightly from one run to the next. This was borne

out by the different values of both σ_i and σ_d when measured at different times. An important parameter affecting those results is the average size of the free-stream nuclei which is known to change significantly even during a single test. Preliminary data obtained using a laser-light-scattering system failed to define the effect of that parameter in relation to normal experimental error as a result of problems with the test system itself [20].

To compare the results of Figure 8 with the available noise theories, Equation (4) was used to describe R_M. Here s_v is assumed to be constant, which seems reasonable after inspecting the pressure distribution curve of Figure 2 for $-\sigma/C_{p_{min}}$ between 0.8 and 0.9. In Equation (4), $\overline{C}_p$ was set equal to $C_{p_{min}} = -1.0$, while the high-speed films and viedotapes showed $C_p = 1/3$ to adequately represent the average pressure experienced by the bubbles during collapse. Employing these values in the classical incompressible noise theory given by Equation (8), a comparison is made in Figure 9 with the empirical $\sigma^{-8.4}$ dependence. For the range of σ observed in this study, the combination of Equations (4) and (8) appear to provide a reasonable model for the functional dependence on σ. However, Equation (8) also predicts the noise per collapse to vary as $V_\infty^{2.4}$ for constant $-\sigma/C_{p_{min}}$, a trend which was not revealed in Figure 8.

Assuming a maximum value for P_g of 0.001 atm and using estimates of R_M from the video tapes, both Equations (11) and (12), after insertion in Equation (15), show cutoff frequencies lying above 100 kHz in the shock wave spectrum. Hence, Equation (16) should be a valid approximation for the two shock wave noise theories. Setting $\overline{C}_p = -1.0$ again in Equation (4) and inserting it into Equation (17), the two theories are compared with the measured trend in Figure 9. These models also show a reasonable correlation to the experimental trends of the noise with σ. Furthermore,

the results indicating that L_c is independent of V_∞ for constant $-\sigma/C_{p_{min}}$ is correctly implied by using the combination of Equations (4) and (17).

Quite possibly, Equation (4) is inadequate for modelling the actual maximum bubble radii observed in this investigation. Using the videotapes, attempts were made to investigate the dependence of R_M on σ and V_∞. Unfortunately, valid results were hampered by difficulties in obtaining radius measurements for any significant range of σ. These difficulties were due to the limited resolution capabilities of the video system in addition to the natural distortion of the bubbles in the flow field. Because R_M is a critical parameter in each of the noise theories, it is thus difficult to arrive at a valid appraisal of any of the models given the uncertainty of this parameter as measured in this investigation. Since no other known studies provide this necessary data, Equation (4) stands as the only functional approximation of R_M, despite its inadequacies.

Energy density spectra of the cavitation noise were found to be flat from 10 to 100 kHz for all values of σ and V_∞. A typical example, after corrections were made for the hydrophone response and tunnel resonances, is shown in Figure 10. The spectra will increase uniformly in level for decreasing σ. Morozov [18] proved that the shape of the cavitation noise spectrum is identical to that of a single bubble collapse when the occurrence of noise bursts follows a Poisson distribution. Studies of the tape recordings indeed showed such a distribution to exist.

Thus, the low-frequency roll-off predicted by Equation (8) was not observed in the spectra. With bubble life times typically around 4 msec, a spectral peak might be expected near .25 kHz such that a roll-off would then be anticipated above 10 kHz. Mellen [11], and more recently Blake et. al. [2], reported an f^{-2} trend at frequencies immediately above the spectral peak which was located near the reciprocal of the bubble life

time. However, the spectra obtained by Blake et. al. appear to rise again to a new plateau following the initial roll-off. Moreover, both Barker [1] and Mellen [11] reported spectra which levelled off after the low-frequency roll-off to a plateau extending from 10 to 100 kHz. Barker also noted that the noise level between 10 and 100 kHz was essentially independent of velocity when σ was held constant, even though it increased as V_∞^6 between 1 and 10 kHz. Although the rate of collapse of individual bubbles was not measured in that study, the data were obtained for incipient conditions where the collapse rates should have been comparable. Nevertheless, Barker's results are also supported by Figure 7.

The presence of a high-frequency spectral plateau implies the existence of pressure pulses, the time constants of which are short compared to the reciprocal of the upper cutoff frequency with spectra described by formulas such as Equation (14). That the noise does not increase with V_∞ for constant $-\sigma/C_{p_{min}}$ in the high-frequency regime seems to support the analysis of Baiter and Esipov and Naugol'nykh if one assumes that the maximum bubble radius depends only on σ. Also, the σ dependence of the noise per collapse is crudely predicted by the shock wave models.

On the other hand, Barker's results suggest that different mechanisms generate noise at low and high frequencies. Both Mellen and Blake et. al. observed spectral behavior supporting the classical model at low frequencies. In addition, the increased velocity dependence at low frequencies reported by Barker is predicted by a comparison of Equation (8) to Equation (17).

CLOSING REMARKS

An attempt was made to suggest appropriate scaling laws for the high-frequency region of travelling-bubble cavitation noise. Although the literature abounds with numerical schemes yielding the sound

radiated from a collapsing bubble, they are not well suited for practical application to flow-induced cavitation. The pressure field described in this study is typical of those associated with many headforms in that the cavitation nuclei experience an abrupt low-pressure impulse that initiates the life cycle of the bubble. Thus, these results should prove helpful in predicting the noise generated by similar headforms used in the travelling-bubble regime. Comparisons with the available noise models would be improved with a study of how the maximum bubble radii depend on the flow parameters such as P_g. Also, phenomena involved in the final stage of collapse require better understanding, as this is the point where sound emission occurs. For instance, thermodynamic effects should be investigated, because such an omission makes even the models employing numerical solutions incomplete.

References

[1] Barker, S. J., "Measurements of Radiated Noise in the Caltech High-Speed Water Tunnel - Part II: Radiated Noise From Cavitating Hydrofoils," Graduate Aeronautical Laboratories, California Institute of Technology, March 1975.

[2] Blake, W. K., Wolpert, M. J., and Geib, F. E., "Cavitation Noise and Inception as Influenced by Boundary Layer Development of a Hydrofoil," Journal of Fluid Mechanics, Vol. 80, pp. 617-640, May 23, 1977.

[3] Harrison, M., "An Experimental Study of Single Bubble Cavitation Noise," Journal of the Acoustical Society of America, Vol. 24, pp. 776-782, November 1952.

[4] Mellen, R. H., "An Experimental Study of the Collapse of a Spherical Cavity in Water," Journal of the Acoustical Society of America, Vol. 28, pp. 447-454, May 1956.

[5] Chahine, G. L., Courbiere, P., and Garnaud, P., "Correlation Between Noise and Dynamics of Cavitation Bubbles," 6th Conference on Fluid Machinery, Budapest, September 1979.

[6] Hentschel, W., "Acoustic and Optical Investigation on the Dynamics of Holographically Generated Cavitation Bubble Systems," Ph.D. Thesis, Third Physical Institute of the Universität, Göttingen, 1979.

[7] Rayleigh, Lord (Strutt, J. W.), "On the Pressure Developed in a Liquid During the Collapse of a Spherical Cavity," Philosophical Magazine, Vol. 34, pp. 94-98, August 1917.

[8] Besant, W. H., Hydrostatics and Hydrodynamics, Art. 158, London: Cambridge University Press, 1859.

[9] Plesset, M. S., "The Dynamics of Cavitation Bubbles," Journal of Applied Mechanics, Trans. ASME, pp. 277-282, September 1949.

[10] Fitzpatrick, H. M. and Strasberg, M., "Hydrodynamic Sources of Sound," 1st Symposium on Naval Hydrodynamics, Publication 515, September 1956.

[11] Mellen, R. H., "Ultrasonic Spectrum of Cavitation Noise in Water," Journal of the Acoustical Society of America, Vol. 26, pp. 356-360, May 1954.

[12] Kirkwood, J. G., and Bethe, H. A., "The Pressure Wave Produced by an Underwater Explosion," National Defense Research Committee of the Office of Scientific Research and Development, Report 588, 1942.

[13] Gilmore, F. R., "The Growth and Collapse of a Spherical Bubble in a Viscous Compressible Liquid," California Institute of Technology, Report 26-4, 1952.

[14] Hickling, R., and Plesset, M. S., "Collapse and Rebound of a Spherical Bubble in Water," Physics of Fluids, Vol. 7, pp. 7-14, January 1964.

[15] Whitham, G. B., "On the Propagation of a Weak Shock Wave," Journal of Fluid Mechanics, Vol. 1, pp. 290-318, 1956.

[16] Baiter, H.-J., "Aspects of Cavitation Noise," Proceedings of Symposium on High Powered Propulsion of Ships, Wageningen, The Netherlands, December 1974.

[17] Esipov, I. B., and Naugol'nykh, K. A., "Collapse of a Bubble in a Compressible Liquid," Soviet Physics-Acoustics, Vol. 19, pp. 187-188, 1973.

[18] Morozov, V. P., "Cavitation Noise as a Train of Sound Pulses Generated at Random Times," Soviet Physics-Acoustics, Vol. 14, pp. 361-365, 1969.

[19] Gates, E. M. and Billet, M. L., "Cavitation Nuclei and Inception," Proceedings of the 10th Symposium of the IAHR, Tokyo, Japan, September 1980.

[20] Hamilton, M. F., "Travelling-Bubble Cavitation and Resulting Noise," Applied Research Laboratory at The Pennsylvania State University, Technical Memorandum No. 81-76, March 1981.

[21] Ivany, R. D., and Hammitt, F. G., "Cavitation Bubble Collapse in Viscous, Compressible Liquids - Numerical Analysis," Journal of Basic Engineering, Transactions of ASME, Vol. 87, Series D, pp. 977-985, December 1965.

[22] Ross, D., Mechanics of Underwater Noise, New York: Pergamon Press, p. 206, 1976.

[23] Fitzpatrick, H. M., "Cavitation Noise," 2nd Symposium on Naval Hydrodynamics, ACR-38, August 1958.

[24] Schiebe, F. R., "Measurements of the Cavitation Susceptibility of Water Using Standard Bodies," St. Anthony Falls Hydraulic Laboratory, University of Minnesota, Report No. 118, February 1972.

[25] Holl, J. W., "An Effect of Air Content on the Occurrence of Cavitation," Journal of Basic Engineering, Transactions of ASME, Vol. 82, Series D, pp. 941-946, December 1960.

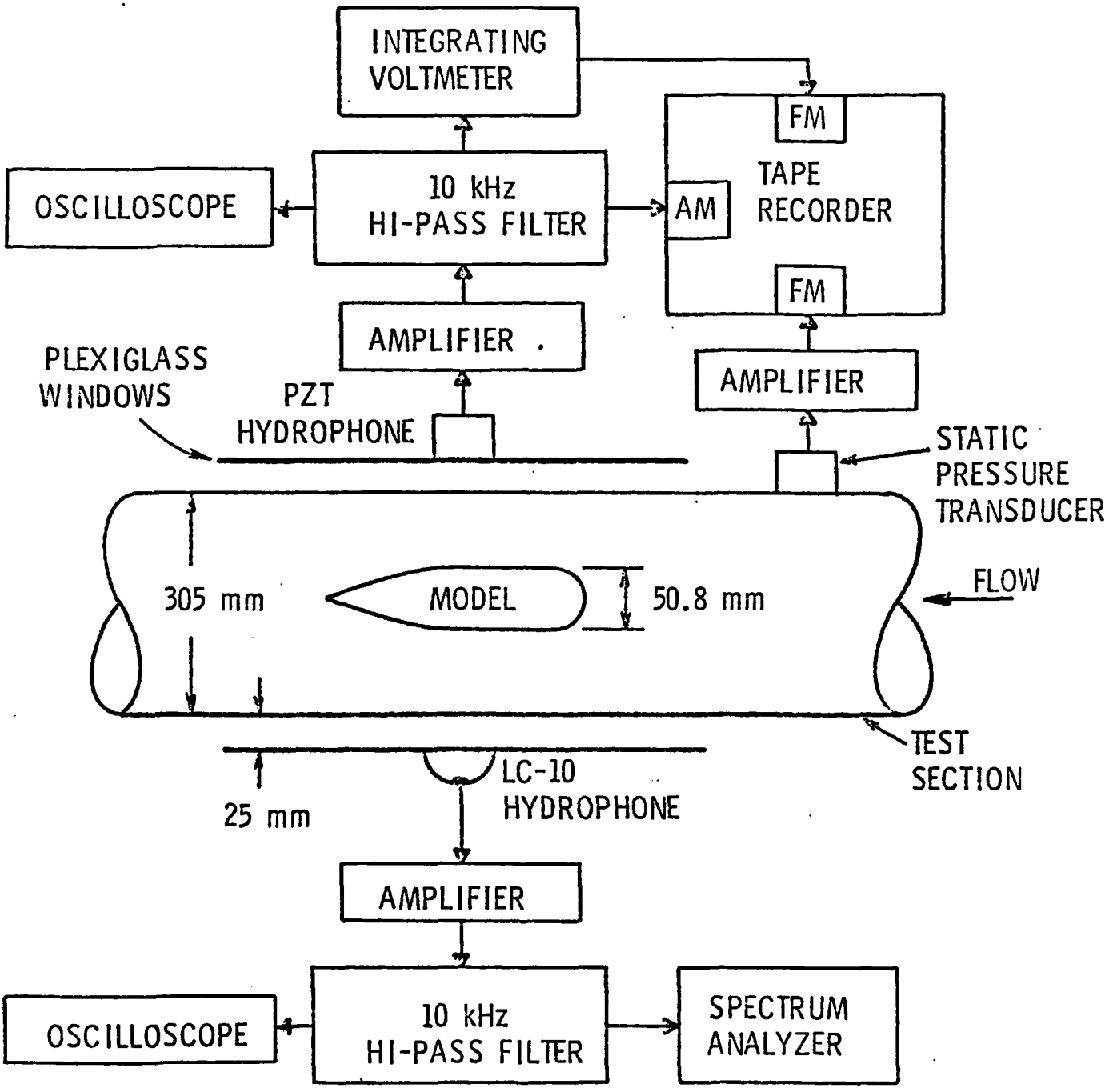
INTEGRATING VOLTMETER
FM
TAPE RECORDER
AM
FM
OSCILLOSCOPE
10 kHz HI-PASS FILTER
AMPLIFIER
AMPLIFIER
PLEXIGLASS WINDOWS
PZT HYDROPHONE
STATIC PRESSURE TRANSDUCER
305 mm
MODEL
50.8 mm
FLOW
TEST SECTION
25 mm
LC-10 HYDROPHONE
AMPLIFIER
OSCILLOSCOPE
10 kHz HI-PASS FILTER
SPECTRUM ANALYZER

Figure 1

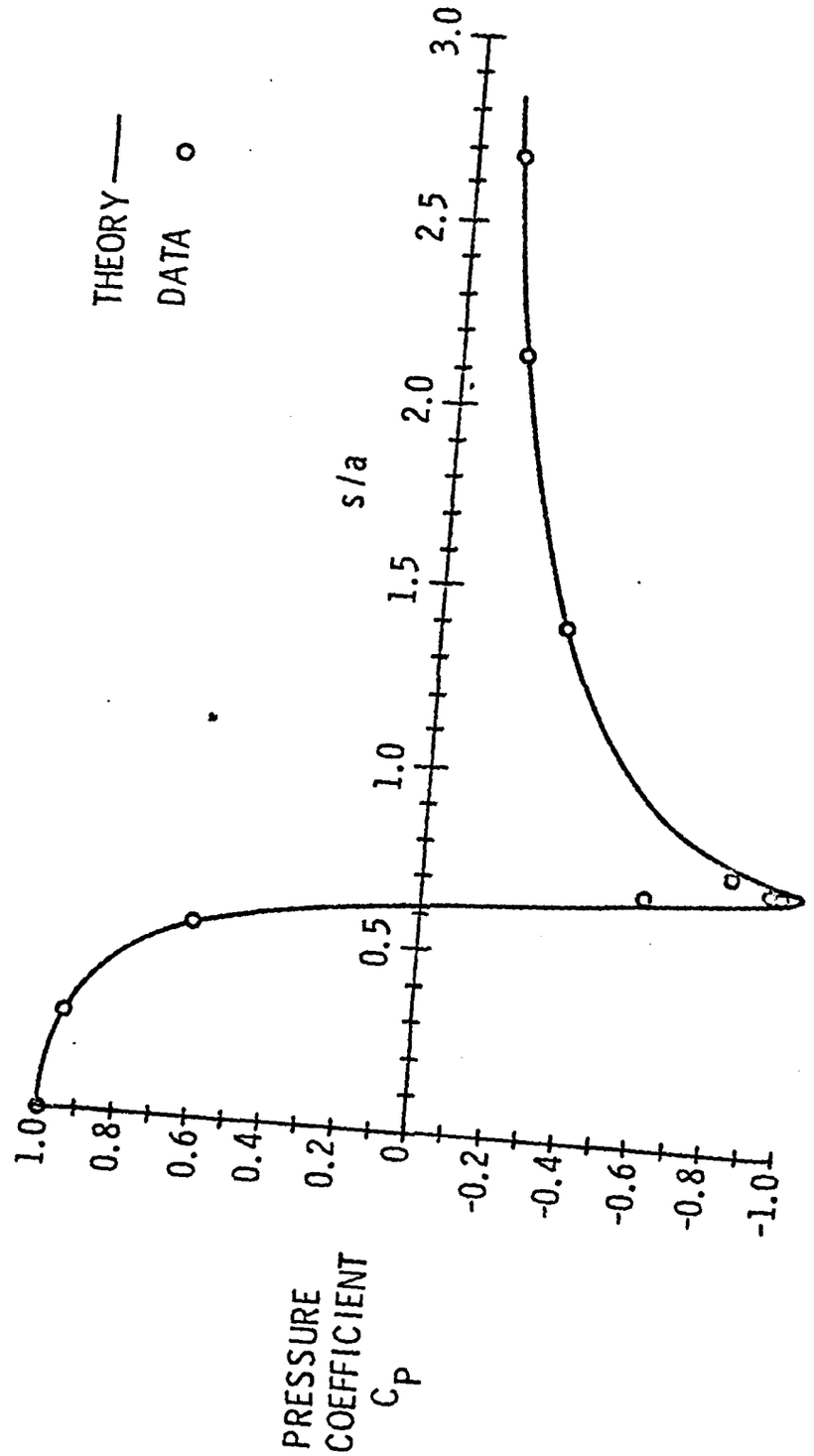
THEORY —
DATA o
s/a
3.0
2.5
2.0
1.5
1.0
0.5
0
1.0
0.8
0.6
0.4
0.2
-0.2
-0.4
-0.6
-0.8
-1.0
PRESSURE
COEFFICIENT
C_P

Figure 2

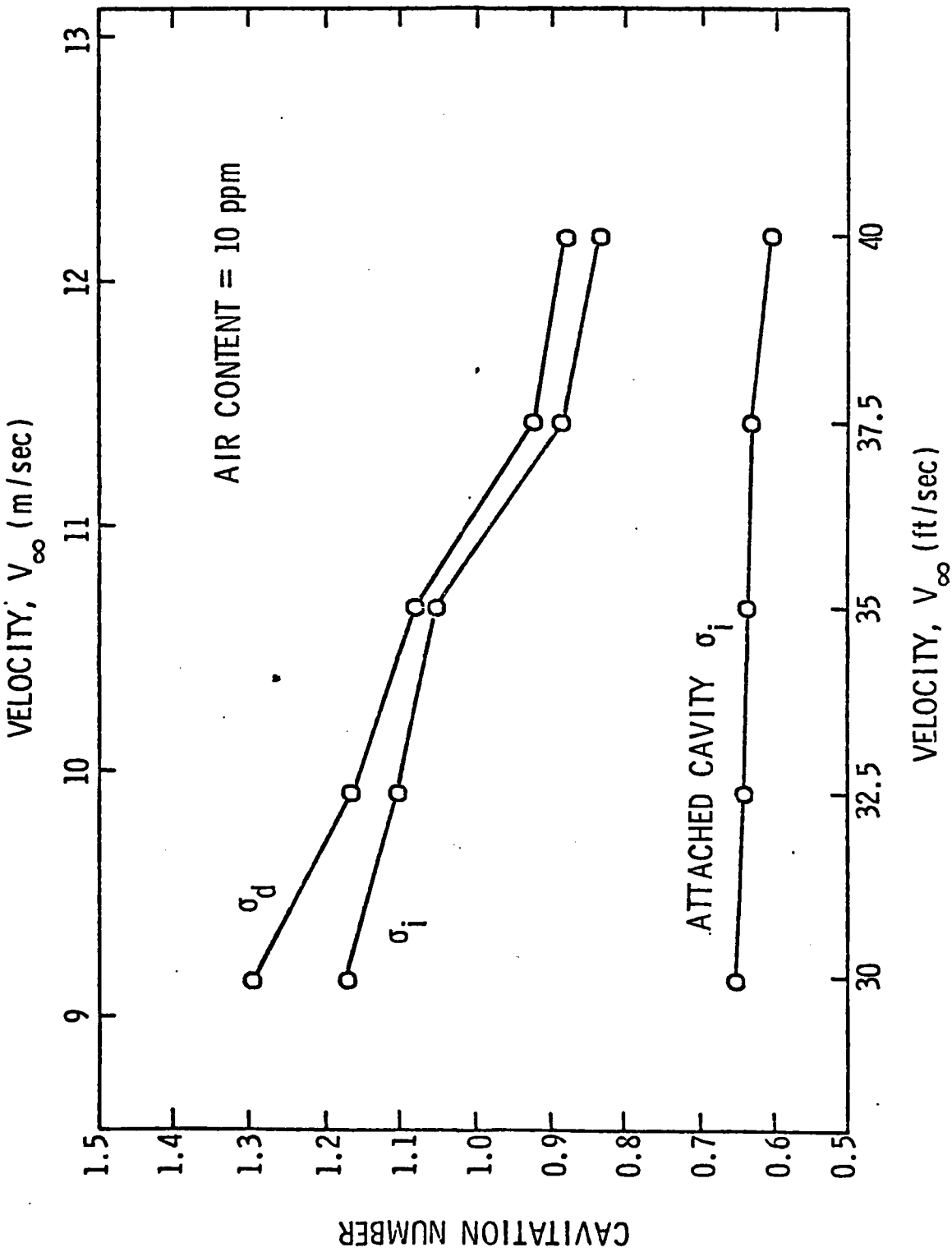
AIR CONTENT = 10 ppm
ATTACHED CAVITY
σ_d
σ_i
σ_i
VELOCITY, V_∞ (m/sec)
VELOCITY, V_∞ (ft/sec)
CAVITATION NUMBER
9
10
11
12
13
30
32.5
35
37.5
40
1.5
1.4
1.3
1.2
1.1
1.0
0.9
0.8
0.7
0.6
0.5

Figure 3

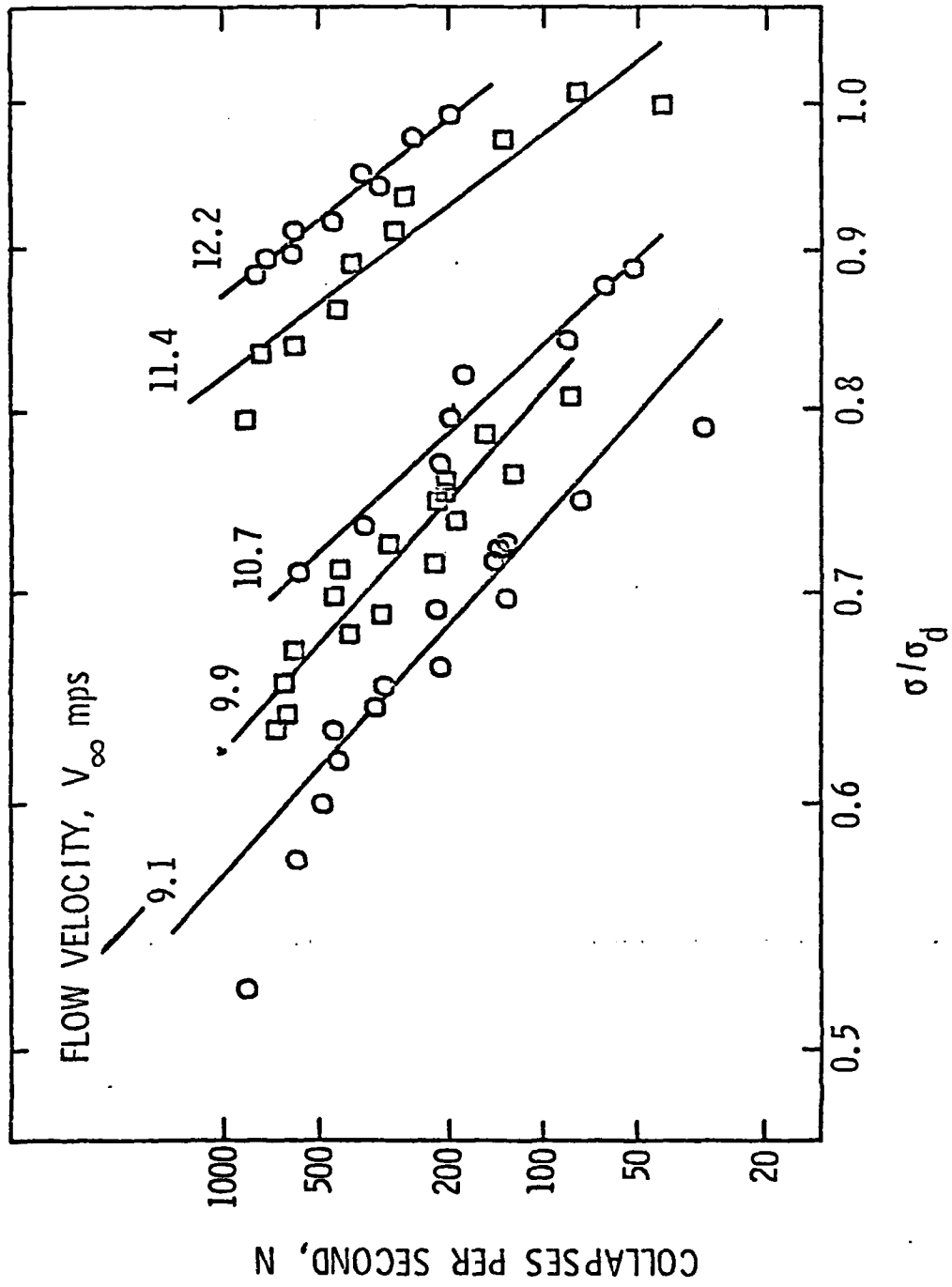
FLOW VELOCITY, V_∞ mps
12.2
11.4
10.7
9.9
9.1
1000
500
200
100
50
20
COLLAPSES PER SECOND, N
0.5
0.6
0.7
0.8
0.9
1.0
σ/σ_d

Figure 4

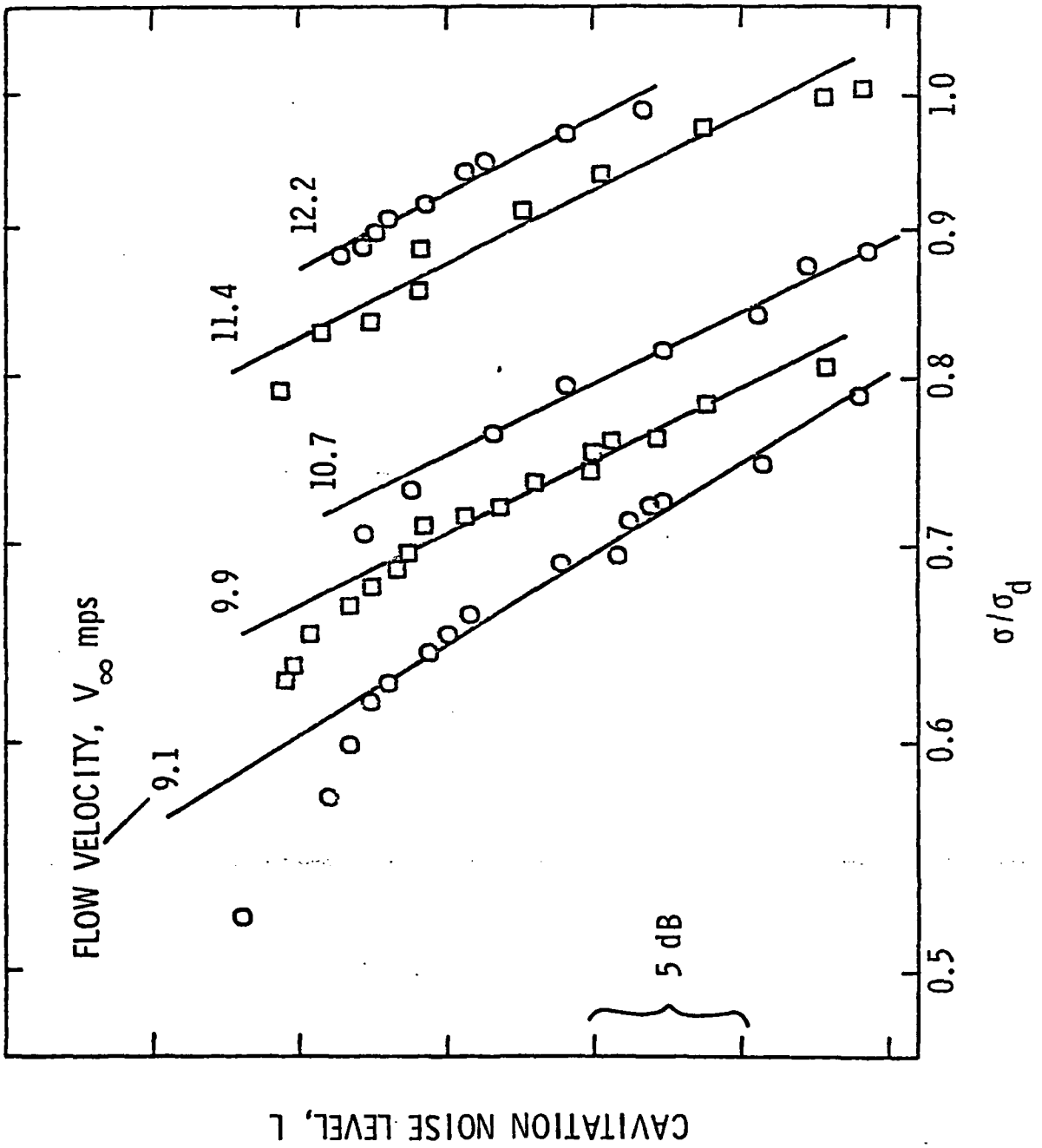
FLOW VELOCITY, V_∞ mps
12.2
11.4
10.7
9.9
9.1
5 dB
1.0
0.9
0.8
0.7
0.6
0.5
σ/σ_d
CAVITATION NOISE LEVEL, L

Figure 5

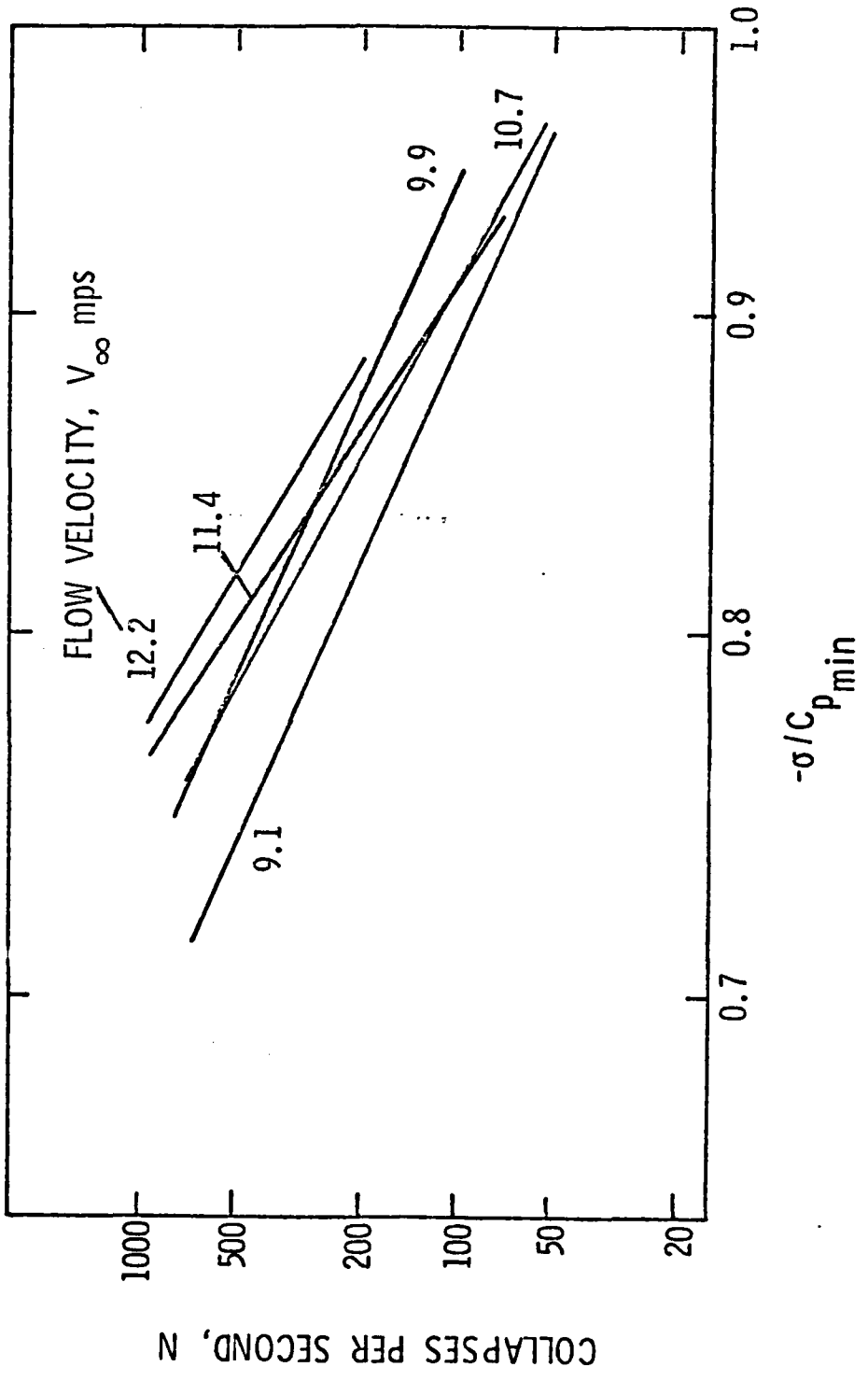
FLOW VELOCITY, V_∞ mps
12.2
11.4
9.9
10.7
9.1
1.0
0.9
0.8
0.7
$-\sigma/C_{p_{min}}$
1000
500
200
100
50
20
COLLAPSES PER SECOND, N

Figure 6

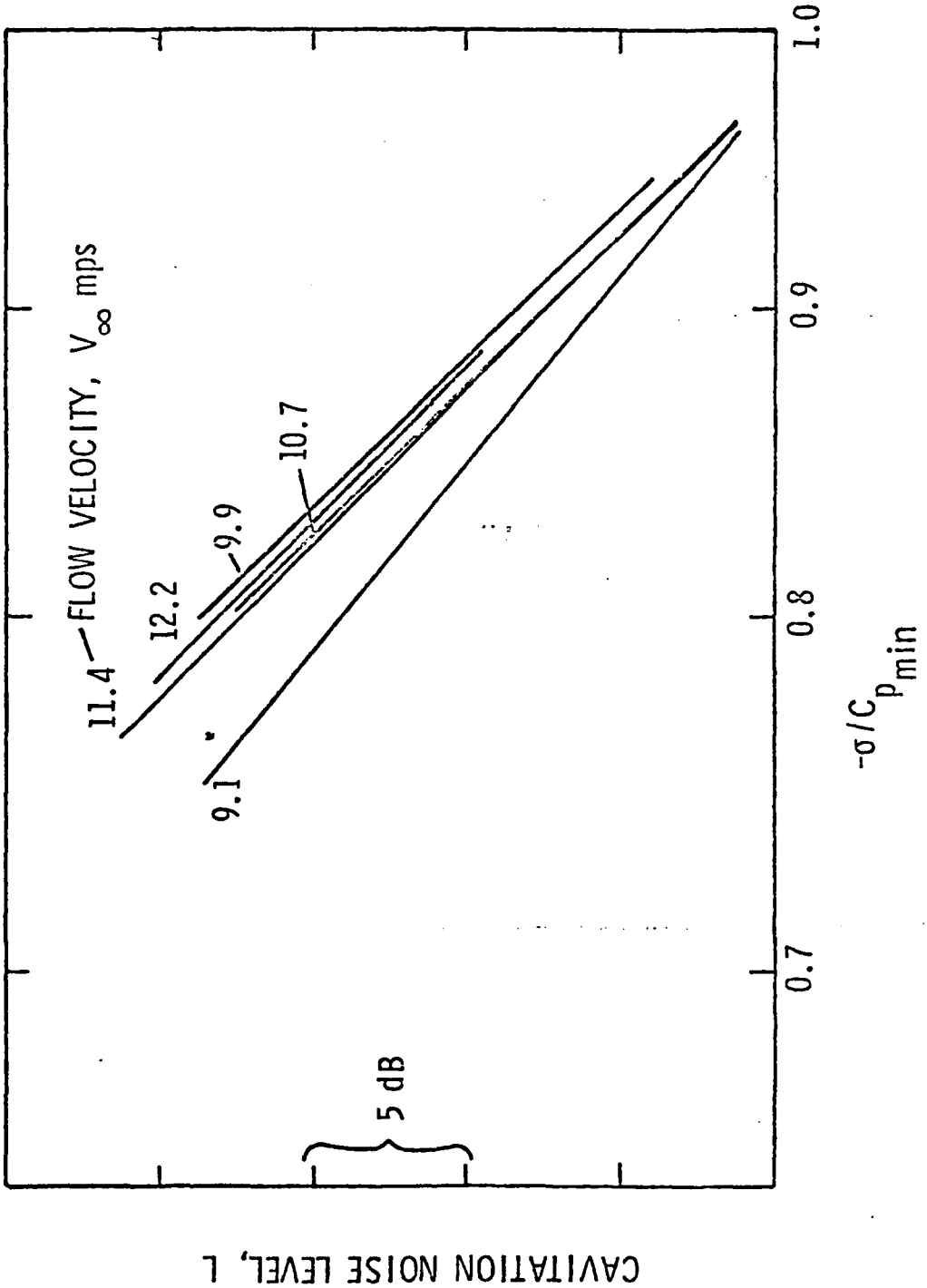
1.0
0.9
0.8
0.7
$-\sigma/C_{p_{min}}$
FLOW VELOCITY, V_∞ mps
11.4
12.2
9.9
10.7
9.1
5 dB
CAVITATION NOISE LEVEL, L

Figure 7

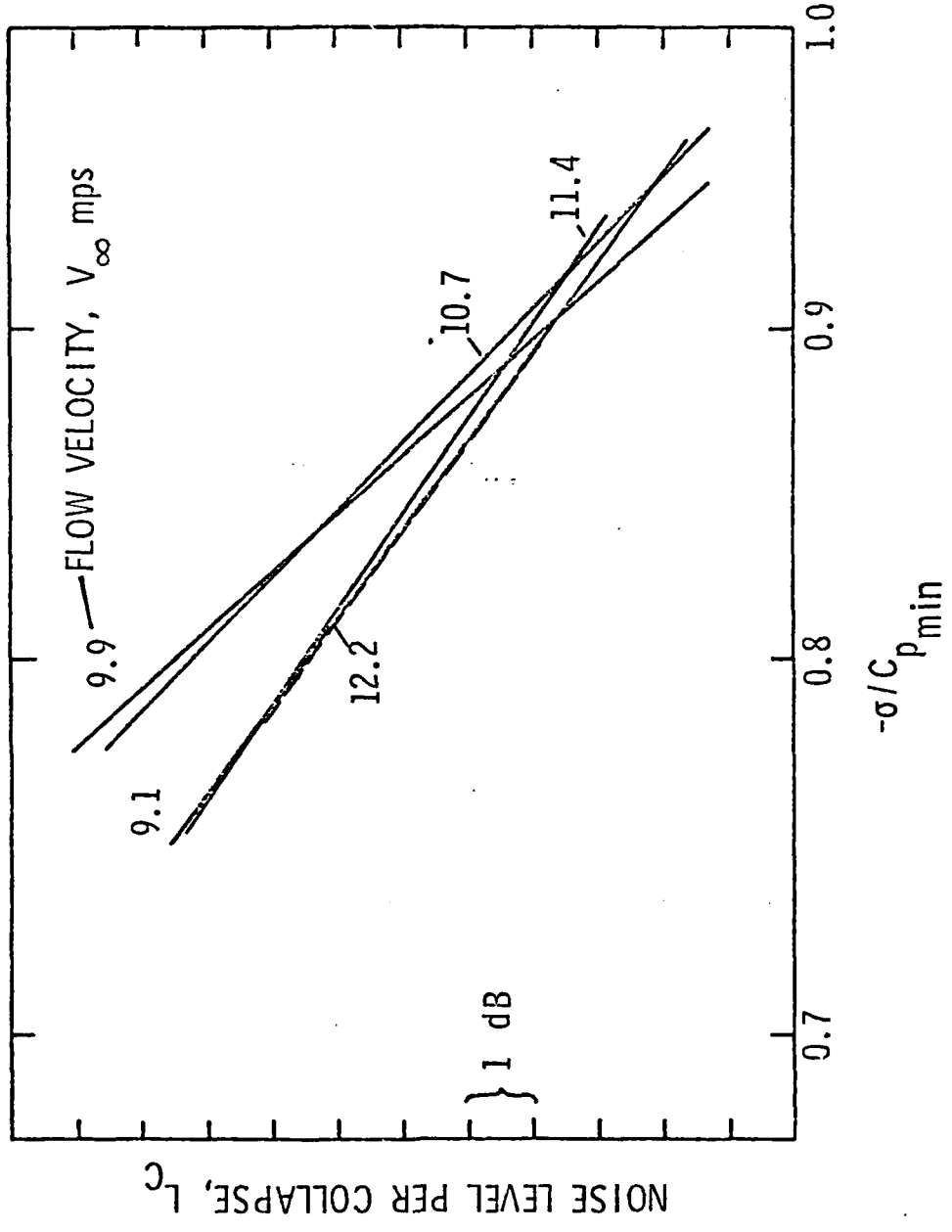
NOISE LEVEL PER COLLAPSE, L_C
1 dB
FLOW VELOCITY, V_∞ mps
9.9
9.1
10.7
11.4
12.2
1.0
0.9
0.8
0.7
$-\sigma/C_{p_{min}}$

Figure 8

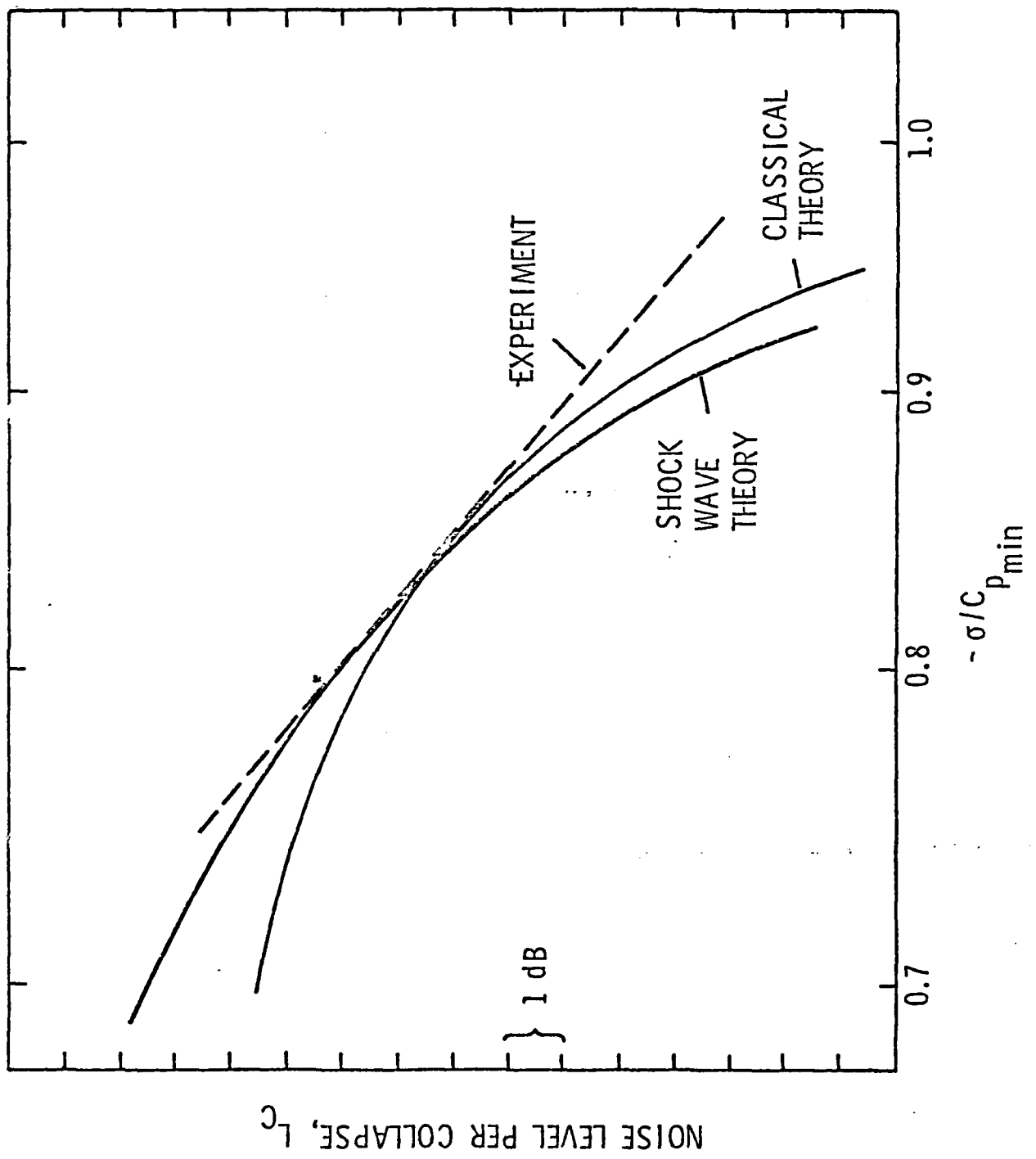
EXPERIMENT
CLASSICAL THEORY
SHOCK WAVE THEORY
1 dB
1.0
0.9
0.8
0.7
$-\sigma/C_{p_{min}}$
NOISE LEVEL PER COLLAPSE, L_C

Figure 9

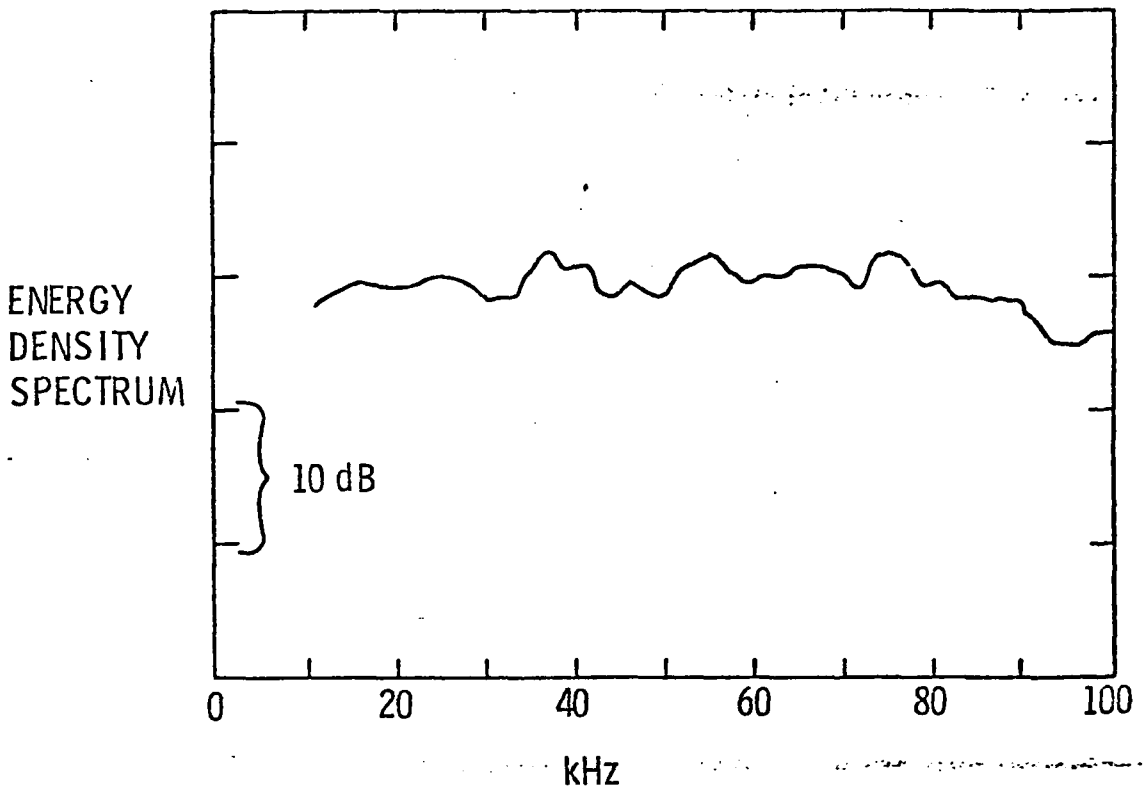

Figure 10

ARL DISTRIBUTION LIST FOR UNCLASSIFIED TM 81-245 by M. F. Hamilton, D. E. Thompson and M. L. Billet, dated 4 December 1981.

Commander
Naval Sea Systems Command
Department of the Navy
Washington, DC 20362
Attn: F. E. Eissing
Code NSEA-05H
(Copy No. 1)

Naval Sea Systems Command
Attn: S. M. Blazek
Code NSEA-05HB
(Copy No. 2)

Naval Sea Systems Command
Attn: A. R. Paladino
Code NSEA-05H1
(Copy No. 3)

Naval Sea Systems Command
Attn: H. C. Claybourne
Code NSEA-05H5
(Copy No. 4)

Naval Sea Systems Command
Attn: F. B. Peterson
Code NSEA-052P
(Copy No. 5)

Naval Sea Systems Command
Attn: F. J. Welling
Code NSEA-521
(Copy No. 6)

Naval Sea Systems Command
Attn: R. Taddeo
Code NSEA-5212
(Copy No. 7)

Naval Sea Systems Command
Attn: T. E. Peirce
Code NSEA-63R31
(Copy No. 8)

Naval Sea Systems Command
Attn: Library
Code NSEA-09G32
(Copy Nos. 9 and 10)

Commander
David W. Taylor Naval Ship R&D Center
Department of the Navy
Bethesda, MD 20084
Attn: Library
Code 1505
(Copy No. 11)

David W. Taylor Naval Ship R&D Center
Attn: K. D. Remmers
Code 1522
(Copy No. 12)

David W. Taylor Naval Ship R&D Center
Attn: R. A. Cumming
Code 1540
(Copy No. 13)

David W. Taylor Naval Ship R&D Center
Attn: J. H. McCarthy
Code 154
(Copy No. 14)

David W. Taylor Naval Ship R&D Center
Attn: T. E. Brockett
Code 1544
(Copy No. 15)

David W. Taylor Naval Ship R&D Center
Attn: R. J. Boswell
Code 1544
(Copy No. 16)

David W. Taylor Naval Ship R&D Center
Attn: T. T. Huang
Code 1552
(Copy No. 17)

David W. Taylor Naval Ship R&D Center
Attn: Y. T. Shen
Code 1552
(Copy No. 18)

David W. Taylor Naval Ship R&D Center
Attn: M. M. Sevik
Code 19
(Copy No. 19)

David W. Taylor Naval Ship R&D Center
Attn: W. K. Blake
Code 1905
(Copy No. 20)

ARL DISTRIBUTION LIST FOR UNCLASSIFIED TM 81-245 by M. F. Hamilton, D. E. Thompson and M. L. Billet, dated 4 December 1981.

David W. Taylor Naval Ship R&D Center
Attn: R. A. Rippeon
Code 1908
(Copy No. 21)

David W. Taylor Naval Ship R&D Center
Attn: R. W. Brown
Code 1942
(Copy No. 22)

David W. Taylor Naval Ship R&D Center
Attn: F. E. Geib
Code 1942
(Copy No. 23)

David W. Taylor Naval Ship R&D Center
Attn: T. C. Mathews
Code 1942
(Copy No. 24)

David W. Taylor Naval Ship R&D Center
Attn: F. S. Archibald
Code 1942
(Copy No. 25)

Defense Technical Information Center
5010 Duke Street
Cameron Station
Alexandria, VA 22314
(Copy Nos. 26 through 31)

Naval Research Laboratory
Washington, DC 20390
Attn: Library
(Copy No. 32)

Netherlands Ship Model Basin
Haagsteeg 2
P. O. Box 28
67 AA Wageningen
The Netherlands
Attn: Dr. Peter van Oossanen
(Copy No. 33)

Netheralnds Ship Model Basin
Attn: Mr. J. van der Kooij
(Copy No. 34)

Naval Postgraduate School
The Presidio
Monterey, CA 93940
Attn: Library
(Copy No. 35)

Fraunhofer-Institut für Hydroakustik
Postfach 260
Waldparkstrasse 41
8012 Ottobrunn
Federal Republic of Germany
Attn: H.-J. Baiter
(Copy No. 36)

Fraunhofer-Institut für Hydroakustik
Attn: Dr. K. Albrecht
(Copy No. 37)

Dr. Ir. A. De Bruijn
Technisch Physische Dienst TNO-TH
Stieltjesweg 1
Postbus 155
Delft
The Netherlands
(Copy No. 38)

F. G. Hammitt
The University of Michigan
Department of Mechanical Engineering
Ann Arbor, MI 48109
(Copy No. 39)

California Institute of Technology
Division of Engineering for
Applied Sciences
Pasadena, CA 91109
Attn: A. J. Acosta
(Copy No. 40)

Professor P. Leehey
Dept. of Ocean Engineering - Room 5-222
Massachusetts Institute of Technology
77 Massachusetts Avenue
Cambridge, MA 02139
(Copy No. 41)

Dr. R. E. A. Arndt
St. Anthony Falls Hydraulic Laboratory
University of Minnesota
Mississippi River at 3rd Ave., S.E.
Minneapolis, MN 55414
(Copy No. 42)

Dr. J. W. Hoyt, Chairman
Cavitation and Polyphase Flow Forum
Department of Mechanical Engineering
San Diego State University
San Diego, CA 92182-0191
(Copy No. 43)

ARL DISTRIBUTION LIST FOR UNCLASSIFIED TM 81-245 by M. F. Hamilton, D. E. Thompson and M. L. Billet, dated 4 December 1981.

Dr. C. S. Martin
Professor of Civil Engineering
Georgia Institute of Technology
Atlanta, GA 30332
(Copy No. 44)

I. S. Pearsall
Head of Fluid Mechanics Division
National Engineering Laboratory
East Kilbridge
Glasgow, SCOTLAND G75 OQU
(Copy No. 45)

E. A. Weitendorf
HSVA Gmblt
Bramfelder Strasse 164
200 Hamburg 60
Postfach 600 929
Federal Republic of Germany
(Copy No. 46)

A. P. Keller
Lehrstuhl für Wasserbau und
Wassermengenwirtschaft
Versuchsanstald für Wasserbau
Technische Universität Munchen
Oskar v. Miller-Institut
D-8111 Obernach, Post Walchensee
West Germany
(Copy No. 47)

Y. Kodama
Ship Research Institute
Ministry of Transport
38-1, 6-chome, Shinkawa, Mitaka
Tokyo, Japan
(Copy No. 48)

T. Sasajima
Resistance and Propulsion Research Lab
Nagasaki Tech. Inst.
Migshusishi Heavy Ind., Ltd.
1-1 Akunoura-Machi
Nagasaki 950-91
Japan
(Copy No. 49)

Dr. V. H. Arakeri
Dept. of Mechanical Engineering
Indian Institute of Science
Bangalore 560 012
India
(Copy No. 50)

Dr. Allen Moore
Admiralty Marine Technology
Establishment
Teddington, Middlesex, TW11 OLN
England
(Copy No. 51)

Admiralty Marine Technology
Establishment
Haslar-Gasport
Hampshire PO122AG
England
Attn: Mr. D. Johnson
(Copy No. 52)

Admiralty Marine Technology Establishment
Attn: Mr. C. Wills
(Copy No. 53)

Mark F. Hamilton
Applied Research Laboratories
University of Texas
P. O. Box 8029
Austin, TX 78712
(Copy No. 54)

The Pennsylvania State University
Applied Research Laboratory
Post Office Box 30
State College, PA 16801
Attn: D. E. Thompson
(Copy No. 55)

Applied Research Laboratory
Attn: M. L. Billet
(Copy No. 56)

Applied Research Laboratory
Attn: GTWT Files
(Copy No. 57)

Applied Research Laboratory
Attn: R. E. Henderson
(Copy No. 58)

Applied Research Laboratory
Attn: J. W. Holl
(Copy No. 59)

Applied Research Laboratory
Attn: D. R. Stinebring
(Copy No. 60)

ARL DISTRIBUTION LIST FOR UNCLASSIFIED TM 81-245 by M. F. Hamilton, D. E. Thompson and M. L. Billet, dated 4 December 1981.

Applied Research Laboratory
Attn: E. G. Taschuk
(Copy No. 61)

Applied Research Laboratory
Attn: R. S. Moyer
(Copy No. 62)

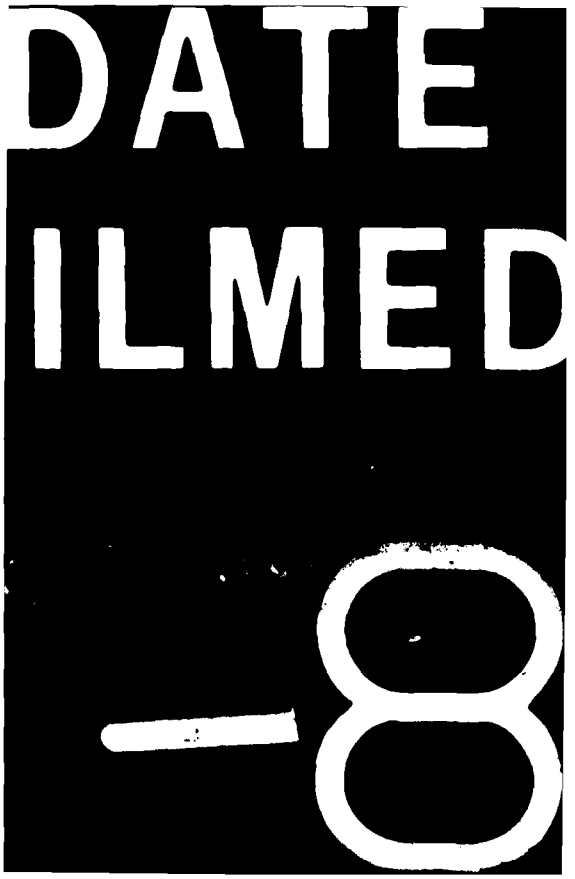
DATE
ILMED
-8